

Advanced manufacturing of thermoplastic tape preforms: braiding simulation, curved preforming, and consolidation via rotational and bladder-assisted molding

Eric Mischorr, Patrick Schaible, Veit Würfel, Johannes Keil, Anton Gelencsér, Sebastian Schabel, Jürgen Fleischer & Maik Gude

To cite this article: Eric Mischorr, Patrick Schaible, Veit Würfel, Johannes Keil, Anton Gelencsér, Sebastian Schabel, Jürgen Fleischer & Maik Gude (2025) Advanced manufacturing of thermoplastic tape preforms: braiding simulation, curved preforming, and consolidation via rotational and bladder-assisted molding, *Advanced Manufacturing: Polymer & Composites Science*, 11:1, 2546292, DOI: [10.1080/20550340.2025.2546292](https://doi.org/10.1080/20550340.2025.2546292)

To link to this article: <https://doi.org/10.1080/20550340.2025.2546292>



© 2025 The Author(s). Published by Informa UK Limited, trading as Taylor & Francis Group.



Published online: 21 Aug 2025.



[Submit your article to this journal](#)



Article views: 279




[View related articles](#)



[View Crossmark data](#)

Advanced manufacturing of thermoplastic tape preforms: braiding simulation, curved preforming, and consolidation via rotational and bladder-assisted molding

Eric Mischorr^a , Patrick Schaible^b, Veit Würfel^a, Johannes Keil^a, Anton Gelencsér^a, Sebastian Schabel^b, Jürgen Fleischer^b and Maik Gude^a

^aInstitute of Lightweight Engineering and Polymer Technology, TUD Dresden University of Technology, Dresden, Germany;

^bInstitute of Production Science, Karlsruher Institute of Technology, WBK, Karlsruhe, Germany

ABSTRACT

Transportation emissions are a major driver of global warming, making vehicle greenhouse gas reduction essential. Lightweight design, such as hollow shafts and tubes, lowers energy use by optimizing stiffness-to-mass ratios. Fiber-reinforced polymers, especially thermoplastic variants, excel in these applications due to their high specific stiffness, customizable mechanical properties, and scalable manufacturing. This study introduces two novel methods for producing braided hollow carbon fiber-reinforced polyamide 6 profiles: rotational molding for straight preforms and bladder-assisted molding for curved preforms. Numerical simulations of braiding were compared to actual braid architectures, revealing both the capabilities and current limitations of the simulation software for tape-based braiding. Analyses included fiber angle, cover factor, and CT-based wall thickness measurements. The potential for increasing consolidation pressure in rotational molding is shown by means of a theoretical analysis. Bladder-assisted molding produced fully consolidated, minimally wrinkled curved profiles, proving the feasibility of manufacturing high-quality curved braided profiles without post-consolidation forming.

ARTICLE HISTORY

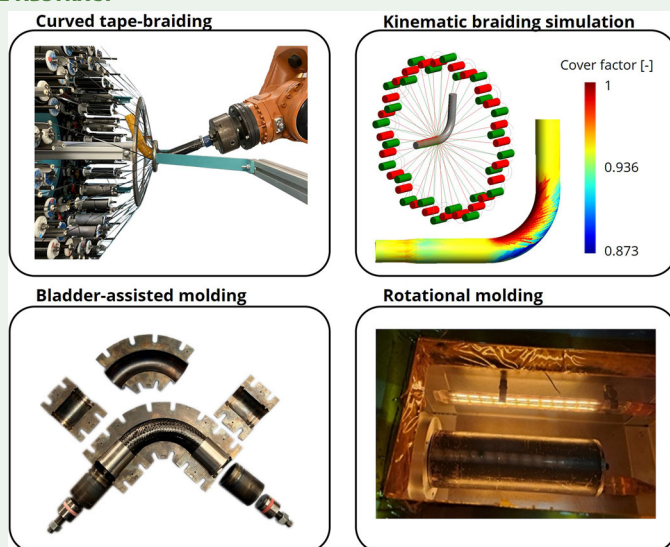
Received 3 June 2025



Accepted 6 August 2025

KEYWORDS

Polyamide-6; rotational molding; thermoplastics; composites; braiding; BraidSim; Bladder-assisted molding

GRAPHICAL ABSTRACT



CONTACT Eric Mischorr  eric.mischorr@tu-dresden.de  Institute of Lightweight Engineering and Polymer Technology, TUD Dresden University of Technology, Holbeinstraße 3, Dresden 01307, Germany

© 2025 The Author(s). Published by Informa UK Limited, trading as Taylor & Francis Group.

This is an Open Access article distributed under the terms of the Creative Commons Attribution License (<http://creativecommons.org/licenses/by/4.0/>), which permits unrestricted use, distribution, and reproduction in any medium, provided the original work is properly cited. The terms on which this article has been published allow the posting of the Accepted Manuscript in a repository by the author(s) or with their consent.

1. Introduction

Transportation and mobility emissions significantly contribute to global warming, making the reduction of greenhouse gases one of the most critical challenges of this era [1]. In mobility applications, reducing weight is a key strategy to lower energy consumption and greenhouse gas emissions during operation. Lightweight components like shafts, tubes, profiles or tension-compression struts are widely realized as hollow structures with closed cross-sections due to their superior stiffness-to-mass ratio when compared to solid material variants. Fiber reinforced polymers (FRP) excel in such applications with highly directional loading directions due to the possibility to orient their reinforcing fibers along the load path. By adapting fiber-reinforced composite designs for tubular sections, component properties like bending or torsional stiffnesses can be locally adjusted using fiber orientation. Optimizing the composite design and advancing manufacturing processes in terms of flexibility and efficiency therefore holds great value and cost-saving potential [2].

Thermoplastic composites offer several advantages, rendering them an attractive choice for the production of structural FRP components in series scale. These advantages include reduced energy requirements during production and better suitability for mass production due to reduced process cycle times [3–5]. Additionally the capability to process the composite parts by reheating them, enables post-forming, reconfiguration or recycling [6]. Consequently, various thermoplastic fiber-reinforced manufacturing processes have been developed. For hollow profiles automated fiber placement (AFP) [7,8], pultrusion [9], shrink tape consolidation [10,11], rotational molding [12,13] and bladder-assisted molding (BAM) [14] are the most common processes. However, each of these processes presents specific challenges that impact achievable component quality, characterized primarily by void content, fiber orientation, and achieved degree of crystallinity [4,5].

Processes such as rotational molding, BAM and shrink tape consolidation require the prior manufacture of a preform – a textile-based semi-finished product. Preforms for hollow structures are typically produced by either winding or braiding fibers onto a mandrel [15]. Winding is characterized by high fiber tension, excellent dimensional accuracy, and a high degree of automation [2]. Braiding, meanwhile, offers additional advantages, including the formation of textile interlacing, which enhances drapeability and allows for the creation of complex structures with high material deposition rates [16]. Pre-impregnated thermoplastic tape materials are the key product for improving cycle times of these process chains, since the additional impregnation processing step during consolidation is not required [2].

There are two main approaches for producing curved thermoplastic FRP-profiles made of braided preforms: reheating and reshaping already consolidated straight hollow profiles – a process that is complicated and can disrupt previously established fiber orientations [17] – or directly producing near-net-shape preforms by braiding on a curved mandrel, which minimizes post-consolidation efforts [18]. Braiding a curved profile can involve variability of braid angles and cover factor due to differences in the distance to the deposition point and roving tensions along the curvature [19]. In order to take advantage of the braiding of near-net-shape preforms, it is therefore necessary to precisely predict the braid architecture resulting from the braiding process. For this purpose, braiding models have been developed which, in a so-called ‘inverse solution’, allow the prediction of the process parameters required to achieve a desired braid architecture [18,20]. In the ‘forward solution’, the braid architecture can be predicted based on the input process parameters [18]. In [21], the inverse solution in the BRAIDSIM software was used to output the axial speed of the braiding machine for overbraiding a pressure vessel. The modeling approach is improved by incorporating a yarn interaction model for the axisymmetric, biaxial braiding process [22] and the simulation of non-axisymmetric geometries or preforms with a curved centerline [18]. An improved yarn interaction model is proposed in [23], enabling the simulation of the biaxial overbraiding process for non-axisymmetric preforms by incorporating the stick-slip effect of interlaced yarns and the friction between yarns and the guide ring. This yarn interaction model was extended to the triaxial braid architecture [24]. In a parametric study, the authors confirmed that the yarn interactions strongly influence the simulated braid angles and convergence zone length of the braiding process. This significantly improved the model’s predictions, especially for overbraiding of mandrels with sudden shifts in cross-section [23,24].

Consolidating textile preforms in BAM enables the production of complex curved profiles utilizing adapted bladder systems [25]. Meanwhile, rotational molding provides a cost-effective alternative for

rotationally symmetric components such as tension-compression struts, with the added benefit of requiring fewer auxiliary materials, such as bladder systems [12,13]. During consolidation, the textile preform expands in diameter inducing fiber loading, thereby optimizing fiber orientation [14,25,26]. A big advantage of BAM and rotational molding compared to other molding processes is the option of using a variothermal mold heating. It allows for controlled heating and cooling rates, ensuring constant and – in case of semi-crystalline thermoplastics – adaptable material properties [26].

This work focuses on the production of high-quality tape-preforms, addressing both straight and curved hollow profiles. First, the capability of numerically designing the braiding process with thermoplastic FRP tapes using the BRAIDSIM software of the University of Twente is investigated. Since the intrinsic bending stiffness of the thermoplastic FRP tapes is neglected in the software, the model accuracy for predicting tape braided architectures is of great interest. Based on the simulation results of a straight tape-braided preform the braiding process is adapted for curved structures, introducing a novel preforming solution for curved tape-preforms. The simulation results are then compared with experimental observations of the braid architecture and the model accuracy is evaluated.

In addition, existing consolidation processes for tape-braided structures are adapted to further enhance manufacturing efficiency. Specifically, rotational molding is applied to straight tape braids for the first time, demonstrating its feasibility for rotationally symmetric structures. Furthermore, blow molding is successfully employed for the first time with curved tape-braided preforms, showcasing its potential as a consolidation method for complex geometries. Through these investigations, this work contributes to advancing the manufacturing processes for thermoplastic tape composites, paving the way for resource-efficient production of advanced hollow profiles.

2. Materials and methods

2.1. Material

In this study, a thermoplastic tape by Celanese is processed in the braiding process. The CELSTRAN[®] CFR-TP PA6 CF60-03 has a Polyamide (PA) 6 matrix, TORAY INC T700S carbon fibers (CF) and a fiber volume fraction of 48%. Detailed information on the PA6 polymer utilized as matrix for the fibers is not available. However, a melting temperature of 220 °C and a glass transition temperature of 57 °C is provided in the data sheet [27]. In Figure 1 an exemplary cross-section of a single tape is shown. It exhibits a consistent thickness of 0.14 mm with matrix-rich surfaces. However, the distribution of fibers and matrix is non-uniform, with fiber bundles remaining distinguishable. The dense packing of fibers results in an insufficient impregnation of the fibers and thus intralaminar voids in the fiber bundles.

2.2. Kinematic braiding simulation by BRAIDSIM

While the braiding of rotationally symmetric profiles can be accurately described using analytical relationships [28,29], the design and characterization of non-symmetric braids is more challenging. Curved

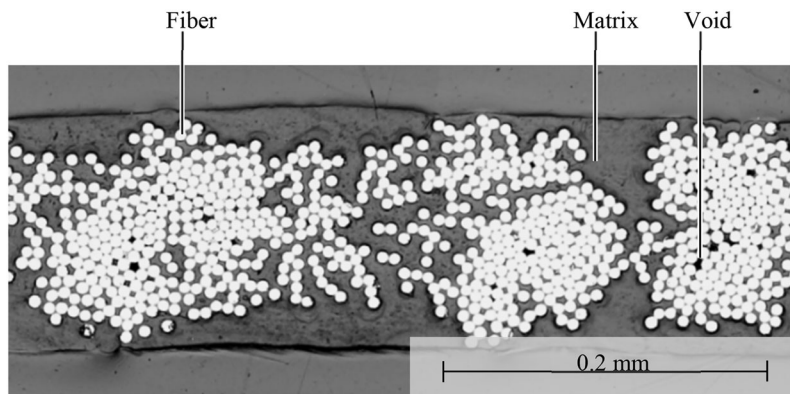


Figure 1. Photomicrograph of the used tape material.

braided hollow profiles, for instance, feature double-curved surfaces that complicate the prediction of fiber orientation and cover factor. Consequently, conventional analytical models prove inadequate, and more advanced methods, such as kinematic simulations, are required to capture the intricate motion and geometry involved. In this work, the kinematic braiding simulation software BRAIDSIM is used to predict the braid angle and the cover factor on the intrados, the extrados and the neutral line of a curved mandrel. Two main inputs are required to run BRAIDSIM. First, a mesh that maps the mandrel's geometry is needed. The geometry of the mandrel is meshed using the GMSH software [30] with 3-node triangle element types and an element size factor of 0.02, resulting in a surface mesh containing 228,146 elements. Second, an input file containing process-specific parameters, such as take-up speed and yarn width, is required. RAVENHORST insightfully describes the functionality and possibilities of BRAIDSIM in detail in [20]. Since BRAIDSIM is based on a kinematic approach, it has computing power advantages over a finite element approach. However, it neglects some effects that occur in a real braiding process. For example, the effects of yarn interactions, such as friction between yarns or between yarn and mandrel during deposition, are not considered yet. Additionally, the mechanical loads on the yarns caused by the bobbins' spring-loaded tensioning system are not considered. These effects can cause fiber entanglement or breakage, which leads to deviations in inter-yarn forces. Ultimately, this influences the braid angle and cover factor [22]. Furthermore, BRAIDSIM does not allow for the use of thermoplastic tapes as semi-finished products. These tapes have a higher bending stiffness than regular yarns, resulting in different deposition behavior during braiding. To evaluate the impact of these model simplifications and determine the accuracy of the model for the curved, tape-based preform, the model results are compared to those of the experimental investigation. Table 1 shows the parameters used for the kinematic simulation. The take up speed and spool rotation speed were calculated based on analytical relationships between process parameters and braid architecture [28,29] and used for the experimental braiding operations as well. There is a difference in the machine setup modeled in the simulation compared to the machine setup used in the experiments. An axial braiding machine (HERZOG, KfH 1/72/48-100) is used for the experimental investigation. Due to collision issues involving the mandrel and the tapes as well as the tapes relatively high flexural modulus, two guide rings have been implemented to deflect the tapes, see Figure 2b. In the experimental setup, the tapes are deflected on the outer radius of the first guide

Table 1. Parameters for the kinematic braiding simulation.

Parameter	Value	Units
Machine radius	390	mm
Number of bobbins	48	pcs.
Mandrel diameter	42	mm
Radius of curvature	101.6	mm
Guide ring – braiding wheel gap	0.3	mm
Guide ring radius	25	mm
Spool rotation speed	22.5	deg/s
Take up speed	9.2	mm/s
Yarn width	3	mm

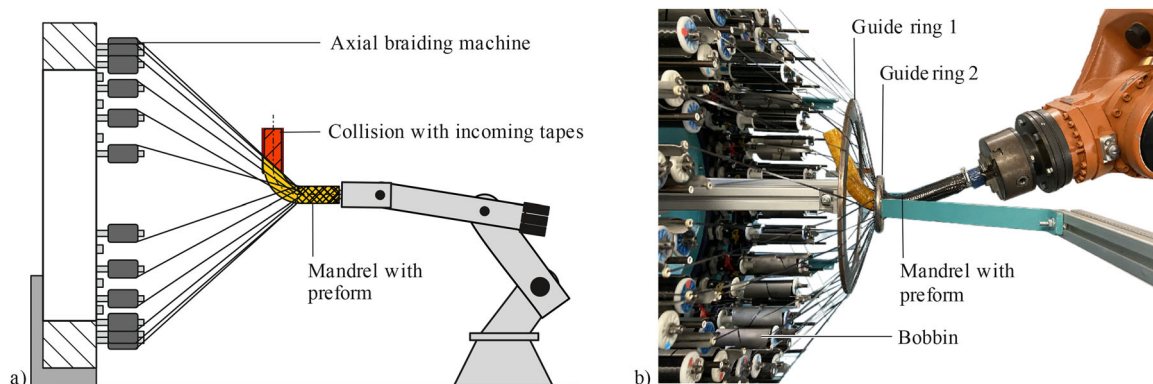


Figure 2. Tape-mandrel collision in a conventional braiding process (a); Double guide ring setup (b).

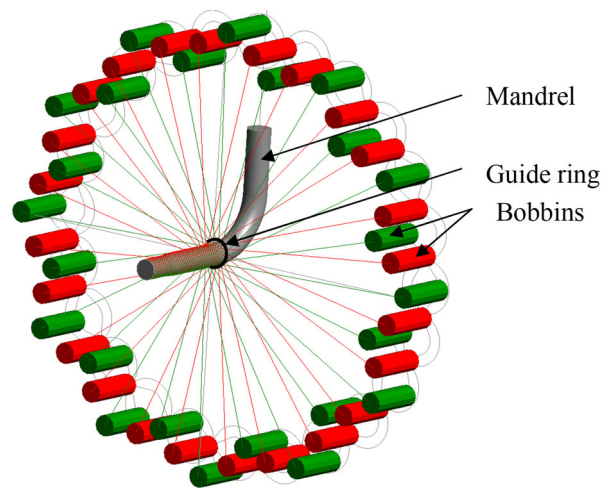


Figure 3. Configuration of the numerical braiding process.

ring ($r_1 = 200$ mm) first and then on the inner radius of the second guide ring ($r_2 = 50$ mm). In BRAIDSIM this configuration of the tape deflection cannot be modeled. By using one guide ring in the center of the braiding machine, proper yarn deposition in the simulation can be ensured. The configuration of the numerical braiding process is illustrated in Figure 3. This configuration is only possible in simulation since the collision of incoming tapes and the mandrel (see Figure 2a) is not an issue in the kinematic model. The radius of the guide ring in the simulation is slightly larger than the mandrel's radius, which enables a uniform yarn deposition.

2.3. Preforming

2.3.1. Straight preforming

A HERZOG KFH 1/72/48-100 axial braiding machine is employed in the fabrication of straight preforms. A distinguishing feature of this machine is the parallel orientation of the spool or bobbin axes relative to the process axis (Figure 2b). The preform's inner surface, and consequently its shape, is determined by the mandrel that is overbraided in the process. For straight preforming, the mandrel is fixed on a KR 210 L180-2 2000 KUKA AG industrial robot, which moves the mandrel along a single axis through the machine. The desired hollow profile has an outer diameter of 40 mm and the laminate structure follows the sequence $[\pm 45^\circ]_8$. This fiber orientation is primarily optimized for torsional load transfer, making it suitable for applications such as drive shafts. A mandrel with a diameter of 34 mm, a braiding wheel configuration with 48 bobbins and tapes with a width of 3 mm are used. The eight layers of the desired preform are braided on to the mandrel and over one another in the process. Therefore, the 'mandrel' diameter of each subsequent braid layer increases. During consolidation the preform expands radially inducing a shear deformation on the braid layers changing the braid angles. The inner braid layers are subjected to a greater shear deformation than the outer layers. Therefore, the initial braiding angle of the preform varies from $\pm 42.1^\circ$ at the inner layer to $\pm 44.8^\circ$ at the outer layer and is different from the final braid angle. With the used set-up, preform lengths of 2 meters were produced. For the subsequent consolidation, the preforms were cut into segments with lengths of 150 mm. To ensure their structural integrity after cutting, each segment was circumferentially welded with a soldering iron on both sides of the cut.

2.3.2. Curved preforming

The manufacturing of a curved hollow profile was developed at the same braiding machine. The desired hollow profile has an outer diameter of 51.1 mm, a laminate architecture of $[\pm 45^\circ]_8$ and features a 90° curvature with a neutral fiber radius of 101.6 mm. Due to the sharp curvature of the mandrel that undercuts the preform, it is impossible to demold the preform from a conventional mandrel without causing damage. Therefore, a lost core approach was chosen, which uses a water-soluble braiding mandrel to demold the preform. The mandrel is additively manufactured using a CREALITY ENDER 5 printer to enable reproducible

fabrication of braiding mandrels. POLYMAKER POLYDISSOLVE S1 filament, a polyvinyl alcohol (PVA)-based material, was selected due to its notable water-soluble properties. To ensure complete dissolution, it is advantageous to rinse water through the entire mandrel, thereby eliminating its structural integrity. The braiding process involves high fiber tension, so adequate intrinsic rigidity during braiding is necessary. Consequently, the braiding mandrel is constructed using a gyroid infill structure—a triply periodic minimal surface that forms a highly ordered, interconnected pore network—to ensure sufficient reinforcement while allowing water to flow through [31]. Alternative infill structures, such as honeycomb or cubic patterns, possess closed-cell designs that hinder uniform rinsing and are therefore not suitable for this application. The additive manufacturing process with an insight view of the mandrel as well as the resulting braiding mandrel are shown in Figure 4. Prior to braiding, the entire mandrel is wrapped with polyimide tape to prevent contamination of the preform during the subsequent dissolution process. The braiding set-up is similar to the braiding of the straight profile. To prevent breakage at the clamping point, this mandrel section is reinforced with a metallic insert, ensuring structural stability during the braiding process.

In order to maintain a constant fiber angle of the preform, the industrial robot navigates the braiding mandrel through a guide ring, ensuring that the cross-section of the mandrel at the deposition point remains parallel to the guide ring. Another challenge during the braiding of curved sections, particularly those with a 90° curvature and additional straight segments, occurs in the form of tape-mandrel collisions, as illustrated in Figure 2a. To address this challenge, the double guide ring configuration depicted in Figure 2b has been devised. This configuration deflects the tapes more steeply, thereby preventing collisions with the mandrel.

2.4. Consolidation processes

2.4.1. Rotational molding

The straight preforms are consolidated using a rotational molding process. The process set up is shown in Figure 5b. The preform is mounted into a one-piece mold and the assembled mold is clamped into a

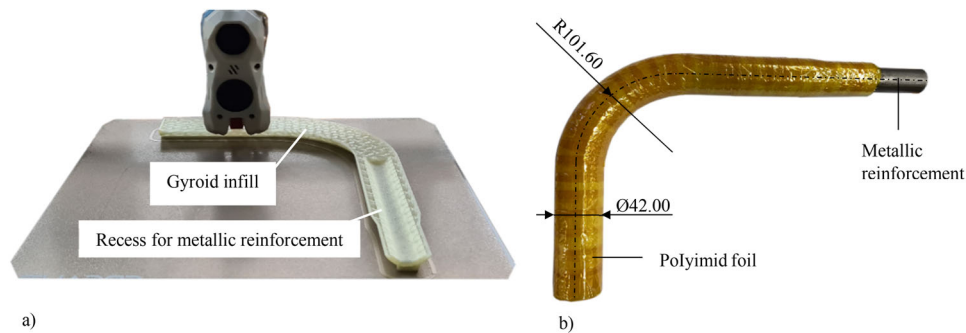


Figure 4. Additive manufacturing process of the mandrel (a); Braiding mandrel (b).

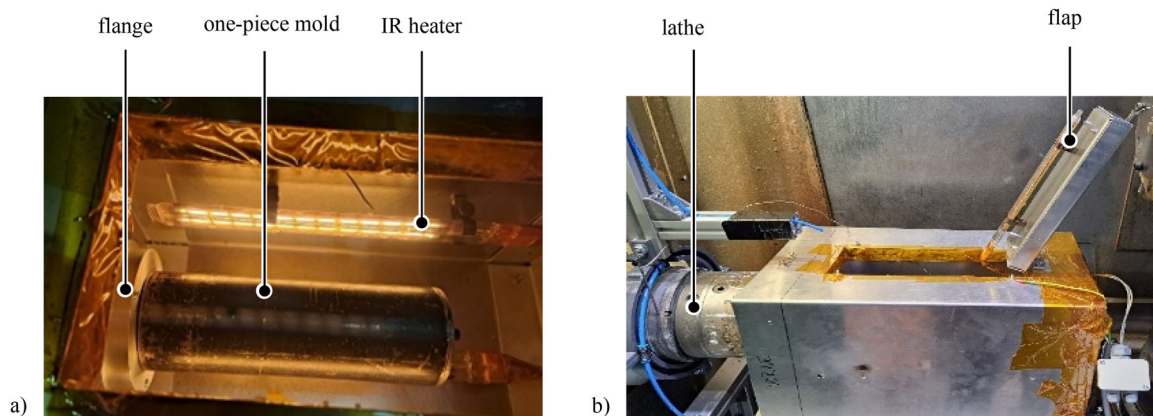


Figure 5. Inside of the heat chamber with flange, tool and one of the four infrared heaters(a); Integration of the heat chamber into the turning center (b).

spindle. In this case a modified INDEX IT 600 turning center with an integrated heat chamber is used. The heat chamber consists of three layers. The innermost and outermost layer are made out of aluminum with a layer of rock wool in between in order to minimize the heat loss during the process. Furthermore, four infrared (IR) heaters with 1.5 kW are mounted into the heat chamber to assure contactless heating and holding of the tool temperature during the process. There is a flap on the top of the heating chamber for inserting the tool. The flap can be operated remotely to control the airflow and as a result control the cooling process. Figure 5a shows the inside of the heating chamber with the mold attached to the flange.

Due to the low consolidation pressure the preform would reach as a result of the centrifugal forces from its own weight, an elastic core is introduced. The elastic core aims to increase the pressure onto the preform and consists of silicon rubber and lead balls with a diameter of 0.6–1.5 mm. The two components are mixed and then casted into a mold with a volume-ratio of 50% of lead balls. After the hardening of the silicon rubber, a small layer of pure silicon around the circumference of the core is applied to reduce the risk of lead balls breaking out and contaminating the inside of the manufactured part. After introducing the core into the mold, the consolidation process starts. CELANESE presents a guideline for press processes for the CELSTRAN[®] CFR-TP PA6 CF60-03 tape [27]. According to this guideline the process cycle for rotational molding was designed. The tool is heated by the IR heaters to a target temperature of 260 °C from room temperature in approximately 10 min. The temperature is held for 10 min in order to achieve a uniform temperature distribution and afterwards the tool is rotated with 3300 rpm leading to a pressure of 0.17 bar. Since the pressure in rotational molding is lower than the pressure specified for the tape in the processing guideline of CELANESE (5.8 bar for 5 min) a longer time under pressure of 20 min was chosen. After maintaining the process conditions for 20 min the flap is opened and the assembly is cooled. By opening the flap, a cooling rate of approximately 10 K/min is achieved. Pressure is maintained until the glass transition temperature of PA6 of 57 °C is reached [27]. Due to the relative low cooling rates, it can be assumed that the final part achieves a high degree of crystallinity, which contributes to its mechanical performance. Figure 6a gives a schematic representation of the process temperature and pressure of the full process cycle. Furthermore, the mold, flange, elastic core and preform are displayed in Figure 6b.

2.4.2. Bladder-Assisted molding (BAM)

The consolidation of curved preforms is performed by BAM. The consolidation tool is shown in Figure 7b. Due to the complex curvature of the preform, a multi-piece tool is employed to facilitate easy demolding after consolidation. The bladder used to apply the consolidation pressure is made of silicone rubber with a wall thickness of 1 mm and a diameter of 35 mm. Silicone is selected for its high elasticity, enabling significant expansion during consolidation without risking bladder failure. The consolidation process follows the temperature and pressure profile illustrated in Figure 7a. The consolidation pressure of 8 bar was selected based on experience, given that the processing guidelines for the PA6 tape outlined in the datasheet [27] are based on a heated platen compression molding process with molding conditions that are not directly comparable to BAM. The consolidation pressure was monitored by means of a pressure gauge and multiple drop tests were implemented during the process cycle to ensure bladder tightness. In order to monitor the

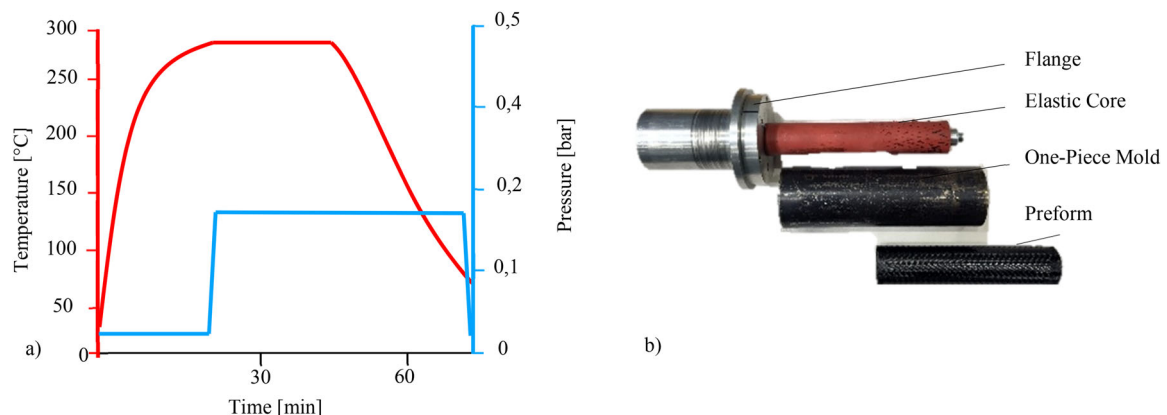


Figure 6. Schematic representation of the consolidation process for rotational molding (a); Molding tool (b).

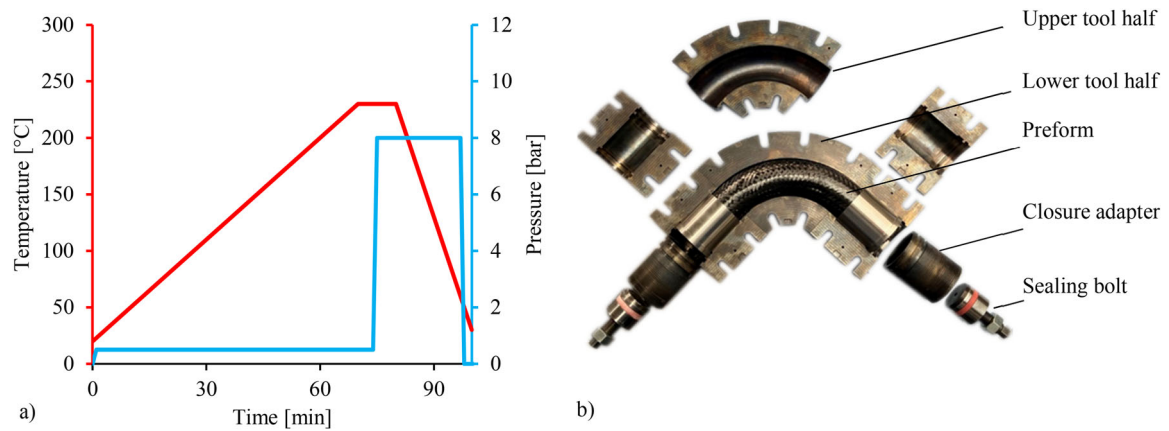


Figure 7. Schematic representation of the consolidation process for BAM (a); Multi-piece molding tool (b).

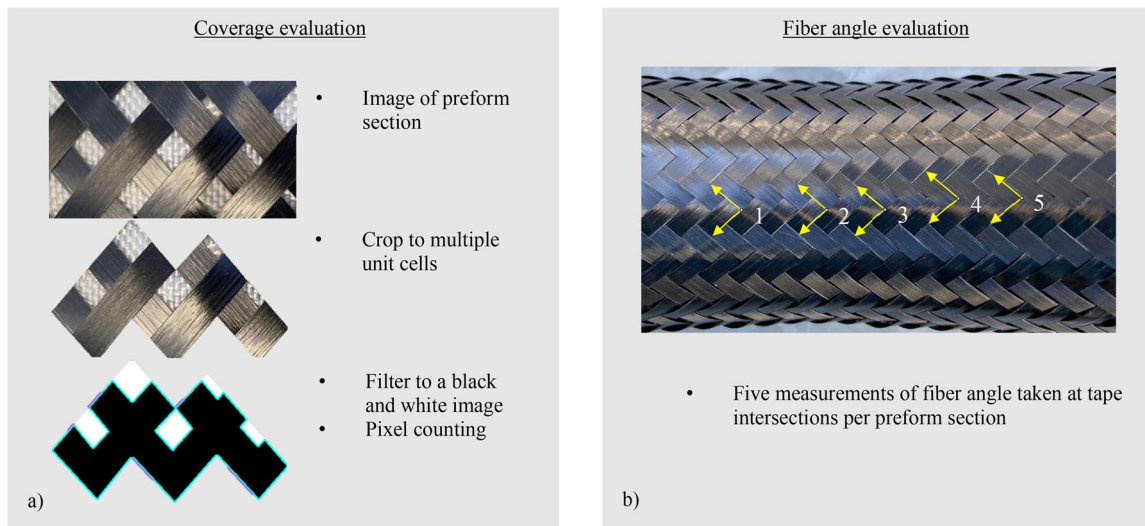


Figure 8. Methods for cover factor evaluation (a) and fiber angle evaluation (b) on the preform.

temperature, holes were drilled in the upper and lower tool half for temperature sensors. Temperature was measured inside the steel tool at a distance of 1.5 mm to the preform. The tape manufacturer specifies a melt temperature of 220 °C for the CF/PA6 tape [27]. To ensure full melting of the preform, the entire tooling assembly is heated to a target temperature of 230 °C at a heating rate of approximately 3 K/min inside a convection oven. A constant bladder pressure of 0.5 bar is maintained during heating, to prevent the preform from collapsing when the matrix polymer begins to melt. Once the target tool temperature is reached, bladder pressure is increased to the consolidation pressure of 8 bar in approximately 30 s. The assembly is cooled at 10 K/min after a hold time of 5 min. The pressure is maintained until the assembly cools down to the tape material's glass transition temperature of 57 °C [27].

2.5. Evaluation methods

The braid angle, cover factor and wall thickness are the main parameters chosen to characterize the quality of the preform and the final composite part. Characteristics, such as braid angle and cover factor, vary from the innermost to the outermost layers of the composite tube. For complex-shaped tubes with curved segments, changes in diameter, or variations in cross-sectional shape, the local differences in braid angle, cover factor, and wall thickness become more intricate and pronounced. To evaluate these parameters, cover factor and fiber angle are visually analyzed at the preform level as shown in Figure 8. Due to the need of high contrast for the analysis of the cover factor, a single layer was braided onto the mandrel wrapped with a white nylon weave. The images are transformed into black-and-white, using

suitable image filtering techniques, enabling the calculation of the cover factor through pixel counting. For the fiber angle measurements, pictures of small preform sections are taken ensuring orthogonal alignment of the camera to the preform surface. A measuring inaccuracy of approximately 1% occurs in this two-dimensional analysis of the 3D surface, due to the curvature of the surface. For each profile section, five measurements were averaged at the tape intersections. Wall thickness measurements of the preform are performed using a vernier caliper by HOLEX with a scale of 200 mm and an accuracy of 1/20 mm. Computed tomography (CT) scanning is employed for the consolidated hollow profiles, as it allows for precise measurement of the wall thickness along the profile axis. The straight tubes, manufactured using rotational molding, were examined at the Karlsruher Institute of Technology – Institute of Production Science (KIT-WBK) using CT on a ZEISS METROTOM 800 with an operating voltage of 120 kV, a current of 160 μ A and an exposure time of 700 ms in a single detector configuration. The scan is analyzed using VGSTUDIO MAX 3.4.5 software by VOLUMEGRAPHICS. The CT scans of the curved hollow profiles, manufactured using BAM, are performed at the Dresden University of Technology – Institute of Lightweight Engineering and Polymer Technology (TUD-ILK) using a PHOENIX V|TOME|X 450 L system, operating at a voltage of 80 kV, a current of 150 μ A, and an exposure time of 500 ms in a single detector configuration. Together, these techniques offer a comprehensive approach to characterizing the textile architecture of braided composite tubes. The results of the experimental evaluation are compared to the results of the numerical braiding process in BraidSim to evaluate the simulation accuracy for braiding with pre-consolidated semi-finished tape products. Furthermore, a comparison between the cover factor of the preform and the resulting wall thickness of the hollow profile is drawn.

3. Results and discussion

3.1. Textile architecture of the straight preform

The straight preform's first braided layer is visually analyzed as explained in chapter 2.5. A simulation of the overbraiding of a mandrel with a length of 1000 mm was performed using BRAIDSIM. As results, the cover factor and fiber angle were extracted for comparison. Figure 9 shows that the predicted fiber angle and cover factor remain constant for the whole length of the straight tube except for one tube ending. This deviation corresponds to the convergence zone of the tapes at the beginning of the numerical braiding process. After about 70 mm the targeted deposition point for the desired braid architecture is set.

The experimental results as well as the simulation results are provided in Table 2. In BRAIDSIM, the resulting braid angle is given for either the warp yarn (designated as 'X Braid Angle') or the weft yarns (designated as 'O Braid Angle'). Since experimentally the fiber angle is determined between the warp

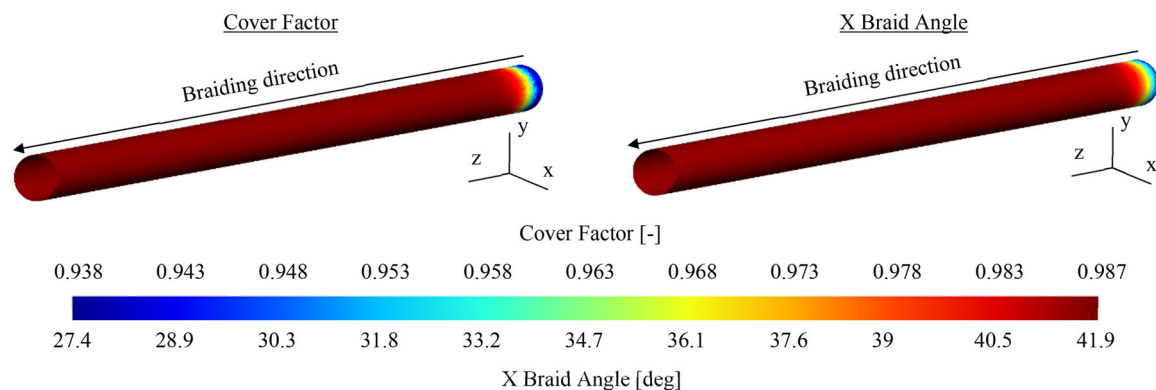


Figure 9. BRAIDSIM simulation results for the first braided layer of the straight preform.

Table 2. Simulated and measured cover factor and fiber angle (mean value and standard deviation).

Parameter	Experiment	Simulation	Deviation
Cover factor	97.16 %	98.73 % \pm 0.002 %	1.62 %
Fiber angle	40.83 \pm 1.29°	41.84° \pm 0.01°	2.41 %

and weft yarn the two fiber angle results in simulation are averaged at every node. The comparative values from simulation were calculated by averaging the results of all nodes on the circumference of a tube segment with a length of 10 mm positioned in the center of the tube. The specified values of the standard deviations of the numerical values correspond to the spread of the results of the selected nodes. The standard deviations specified for the measured fiber angle correspond to the spread between the five measurements. The cover factor was determined using one representative cutout. Therefore, no standard deviation could be calculated. However, this measuring method averages the braid architecture over the selected cutout area. The simulation is in good agreement with the experiment with deviation of the predicted cover factor by 1.62% and of the predicted fiber angle of 2.41%.

3.2. Textile architecture of the curved preforming

For curved preforming, the first braided layer is visually analyzed using photographs taken at the extrados, intrados and neutral line of the curvature. An increase in the cover factor between the extrados and the neutral line is noticeable and is even more obvious in comparison to the intrados, where full coverage has been achieved. In the transitional area between the straight and the curved section of the preform, depicted in Figure 10, an out-of-plane bending of the tapes from the mandrel surface can be observed (scale effect). Depositing two-dimensional tape materials flat on a double-curved surface requires a certain shear deformation of the tapes that is impeded by their stiffness. Consequentially, the tapes deviate from their targeted deposition path resulting in local changes of the braid architecture.

The cover factor and fiber angles of the curved preform are measured at the positions shown in Figure 11 and compared to the numerical results from BRAIDSIM (See Figure 12).

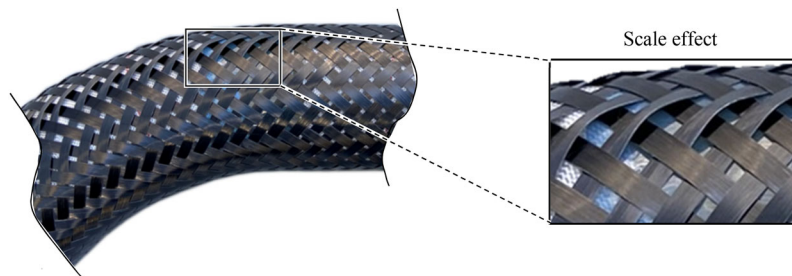


Figure 10. Scale effect observed on the first braided layer of the curved preform.

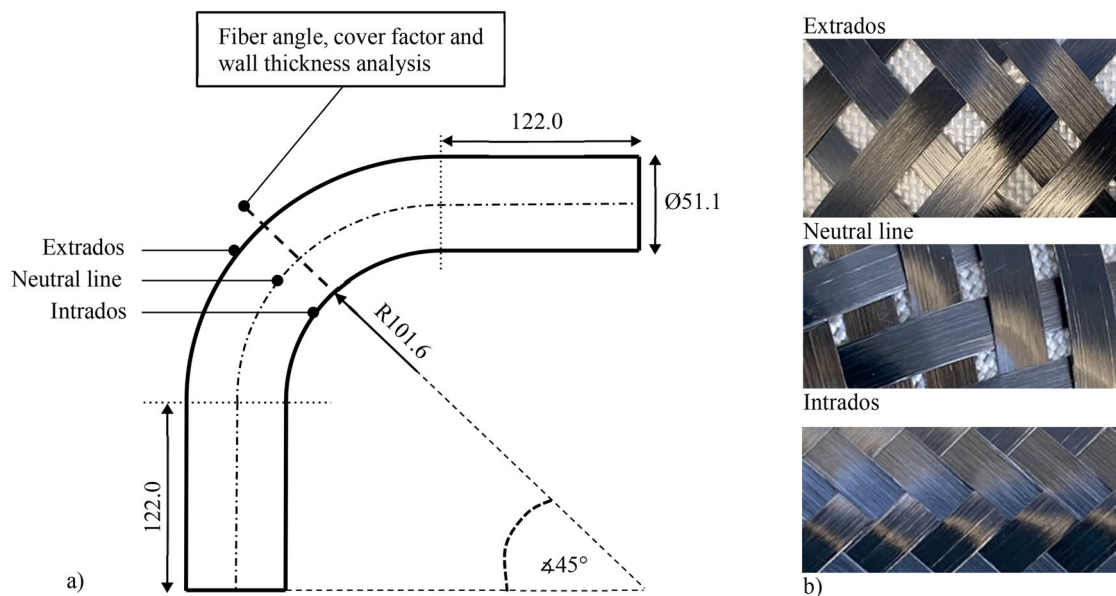


Figure 11. Nomenclature of the curved profile section with dimensions in millimeters (a); Preform images for visual analysis (b).

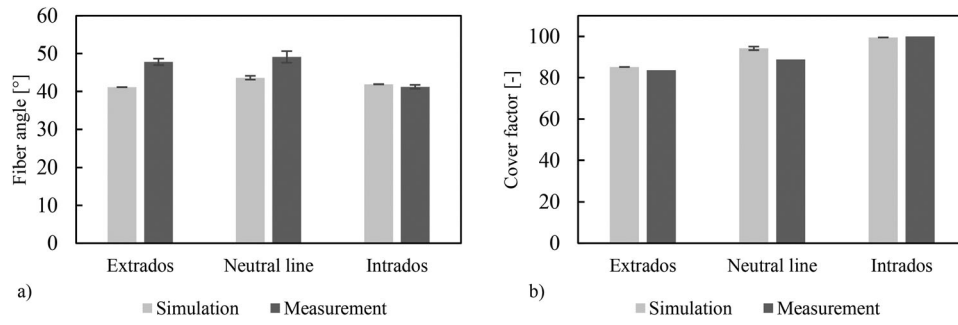


Figure 12. Comparison of model predictions and measurements of the curved preform for fiber angle (a) and cover factor (b).

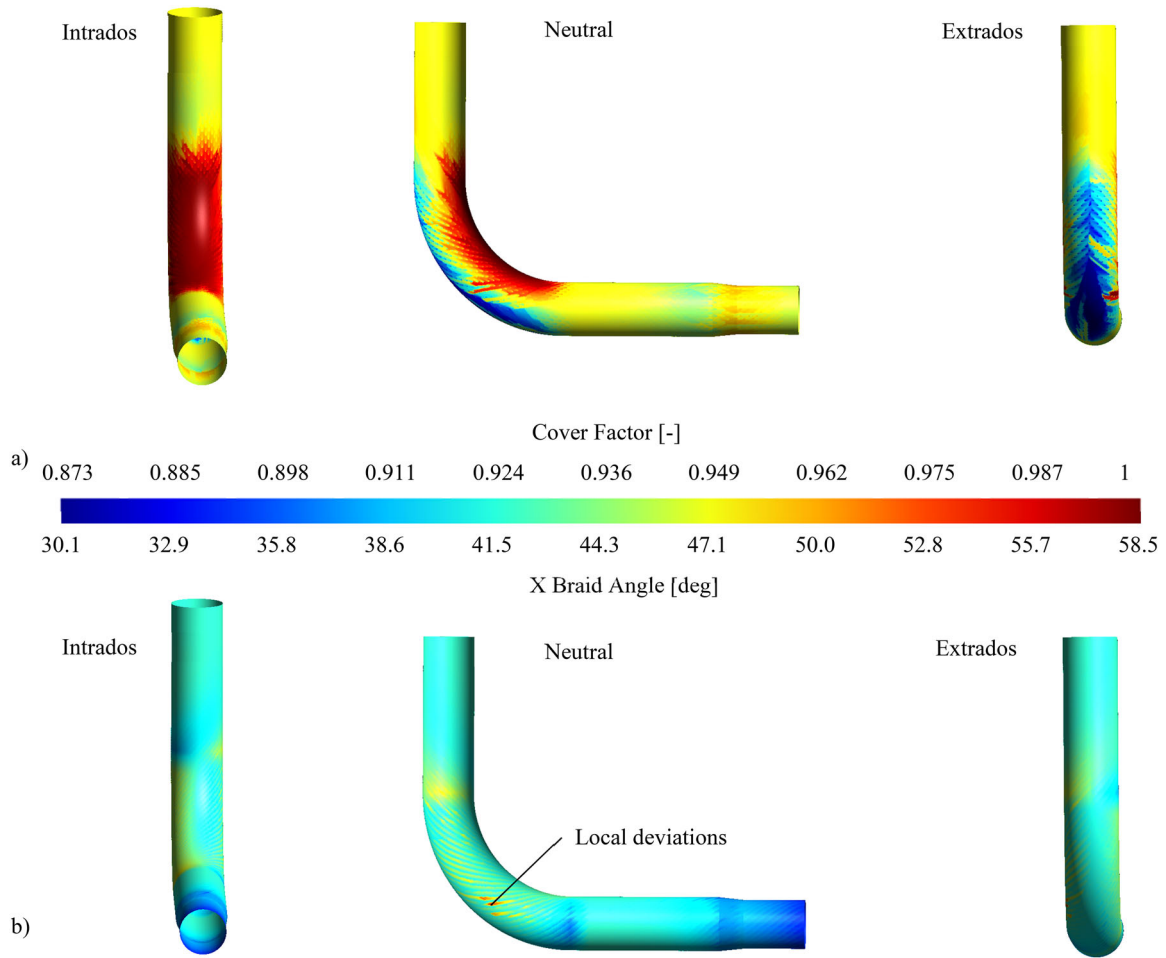


Figure 13. Results of the BRAIDSIM simulation for the first braided layer: Cover factor (a) and braid angle (b).

The plots of the cover factor and braid angle of the kinematic simulation for the first braided layer can be seen in Figure 13.

The results of a targeted selection of nodal groups along the profile axis and circumference were averaged at the desired preform positions. An averaging region of approximately 2 mm^2 was defined at the extrados, neutral line, and intrados at the cross-section specified in Figure 11. By avoiding the inclusion of the nodes with significant local deviations (See Figure 13) representative values could be obtained. The local deviations of the braid angle are due to numerical issues and were designated as numerical noise by [21]. A mesh refinement did not improve the numerical issues. The cover factor exhibits a maximum value on the intrados of 99.5%. It gradually decreases towards the extrados, at which point it attains its minimum value of 85.2%. The resulting braid angle deviates at the cross-section and has its maximum of 43.6° on the

neutral line. It gradually decreases toward the intrados, reaching a value of 41.9° , as well as toward the extrados, where the simulation predicted the minimum value of 41.1° . In Figure 12, a comparison of the experimentally measured data and the results from the BRAIDSIM simulation is shown. The standard deviations are calculated analogous to the approach described for the straight tube. The simulation results demonstrate a good agreement with the experimental data, with a maximum deviation of the cover factor from the measurements of approximately 5%. Cover factor predictions at the intrados closely match experimental observations, indicating full coverage. However, the simulation tends to overestimate the cover factor at the extrados and neutral line. The predicted trend of a decreasing cover factor from the intrados through the neutral line to the extrados aligns well with experimental observations. Both simulation and experimental results indicate that the maximum fiber angle is located on the neutral line. Nevertheless, the simulation underestimates fiber angles at the extrados and neutral line by approximately 11–14%, whereas the predicted fiber angle at the intrados closely matches the measured value. Notably, the measurement revealed a substantial decrease in fiber angle from the neutral line toward the intrados, a trend that is not captured by the simulation.

A possible explanation for the discrepancies between the simulation and experimental results is the omission of the tapes' intrinsic stiffness, since BRAIDSIM was developed for yarn-based braiding, in which bending stiffness is typically negligible [22]. Depositing two-dimensional tape materials flat on a double-curved surface requires a certain shear deformation of the tapes that is impeded in practice by their stiffness. This leads to an arising of the tapes resembling a scale pattern (see Figure 10). Qualitatively, the trends of cover factor and fiber angle of a curved braided preform could be predicted. However, utilizing BRAIDSIM as a process design tool for curved braiding in combination with tape materials requires further investigation. One area for future research is identifying ratios of mandrel curvature to diameter in geometric sensitivity studies at which BRAIDSIM simulations are accurate. Applying the improved yarn interaction model for yarn-yarn and yarn-guide ring friction in non-axisymmetric overbraiding could also significantly improve the model predictions as already shown in [23,24]. To enhance the accuracy of fiber architecture prediction in curved braiding processes, an alternative approach involves applying FEM methods that incorporate the intrinsic bending stiffness of the tapes [32].

3.3. Rotational molding

The straight profiles were visually inspected immediately after demolding. The external appearance of the component is largely homogeneous (see Figure 14). The individual UD tapes of the preform are clearly visible and no changes in the fiber angle can be observed. There is an incompletely molded area in the center of the component around its entire circumference (See Figure 14b). In this area a sealing would have been placed in a thermoset process since the tool was used for parts with a thermoset

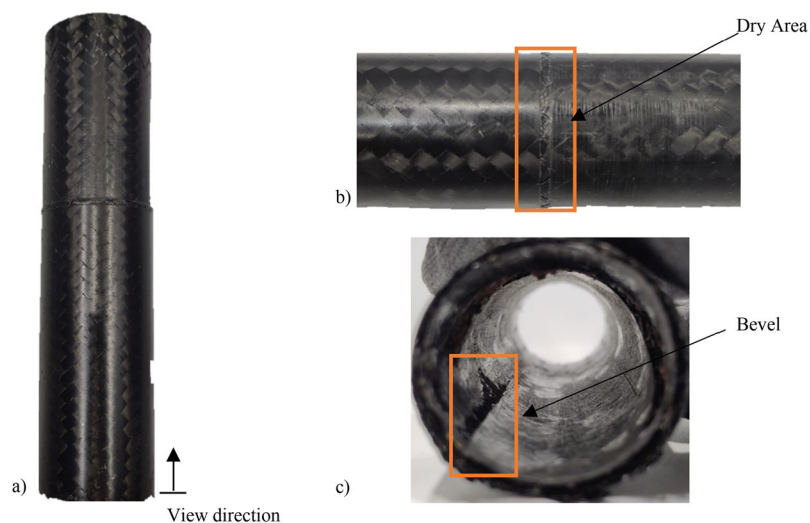


Figure 14. Overall view of the manufactured straight profile (a); Close-up of the dry area at the sealing point (b); View of the inner part of the profile (c).

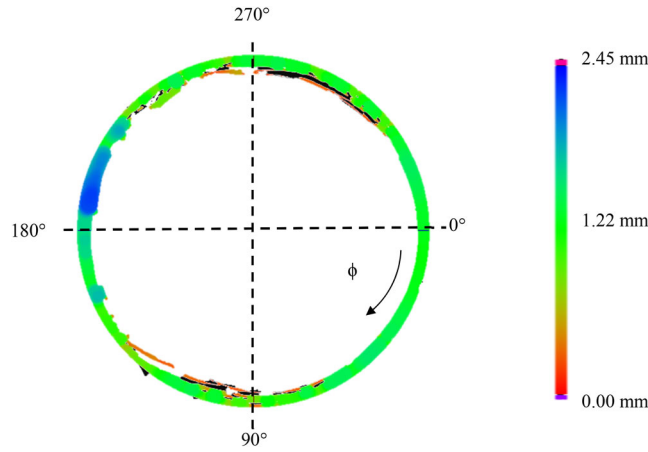


Figure 15. Cross-section of the straight tube from a CT scan for wall thickness analysis.

matrix in the past. The surface defects are therefore caused by the tool and are not considered critical. Partial consolidated areas in the UD tape intersections of the braid are visible at the surface of the component.

The cause can be process-related due to a lack of pressure and as a result of insufficient consolidation. A smooth surface has formed on the inside of the component due to the outside of the elastic core. Furthermore, an impression of the seam of the core is visible. In Figure 14a a complete image of the component is depicted. The profile section containing the dry area caused by the mold seal is visible in Figure 14b. The course of the UD tapes is also clearly visible. Figure 14c shows the inside of the hollow profile with a small bevel along the axis that is molded of the manufacturing related seam of the elastic core. The wall thickness was evaluated from the CT scan depicted in Figure 15. In large parts of the component, there is a compaction of the preform from an initial wall thickness of 2.5 mm to 1.22 mm. The maximum observed wall thickness after consolidation is 2.21 mm, indicated in dark blue, and the minimum observed wall thickness is 0.83 mm, indicated in green in Figure 15. Nevertheless, there are some anomalies in the wall thickness measurement. At 190° position, the scans show a thicker wall area with a wall thickness of about 2 mm. Furthermore, there is a lack of consolidation of the innermost layer in the range of 90–135° and 270°–315°. The innermost layer has no intimate contact with the rest of the laminate. The symmetry of the delamination around 90° and 270° suggests that the pressure distribution in the process was not homogeneous. Possible causes for the inhomogeneous results may be an uneven distribution of the pressure due to inhomogeneities in the elastic core used. This problem could be addressed by optimizing the manufacturing process of the elastic core. Furthermore, the lack of consolidation of the innermost layers indicates a lack of consolidation pressure in the rotational molding process. By increasing the rotational speed an increase in pressure would be achieved but due to limitations of the available machinery this was not possible.

In the following, the pressures within the centrifugal process will be discussed further. The calculation of the resulting pressure from the centrifugal force of the preform and the elastic core is briefly explained below. For this, the Lamé-Navier equation is coupled with the deformation tensor and Hooke's generalized law. The pressure of the core Δp_c is caused by the elastic core at the interface between core and the preform as a result of the centrifugal forces with the angular velocity $\omega = n/(2\pi)$ assuming that the preform is rigid [33]. The elastic core has a young's modulus E_c which is determined by the shore hardness via an empirical relation [34], a poison's ratio ν and a density ρ_c . The resulting pressure of the elastic core Δp_c is represented in a normalized form by the expression in Equation 1 and allows the calculation of the pressure for any cylindrical geometry and material

$$\Delta p_c = \rho_c \cdot R_{c,o}^2 \cdot A^\circ \left(\frac{\omega^2}{4} \left(2\nu_c^2 + 2(1 - t_c^*)^2 \nu_c^2 + \nu_c - (1 - t_c^*)^2 \nu_c - 1 - 3(1 - t_c^*)^2 \right) - M(\sqrt{\varphi_f R_{f,i}^*} - 1) \right). \quad (1)$$

M expresses the dimensions index shown in Equation 2 while factor A° is based on the poison ration ν and normalized wall thickness t_c^* expressed in Equation 3

$$M = \frac{E_c}{\rho_c \cdot R_{c,o}^2}, \quad (2)$$

$$A^\circ = \frac{t_c^*}{2v^2 + t^*(v+1) - 2}. \quad (3)$$

The normalized inner radius of the preform $R_{f,i}^*$ is given by

$$R_{f,i}^* = \frac{R_{f,i}}{R_{c,o}} \quad (4)$$

and the normalized wall thickness t_c^* of the core is expressed by

$$t_c^* = \frac{R_{c,o} - R_{c,i}}{R_{c,o}}. \quad (5)$$

The outer radius $R_{c,o}$ of the core in this work is selected to be 17 mm which is a little smaller than the inner diameter $R_{f,i}$ of the preform. This is to ensure smooth assembly in the preparation of the mould with maximum pressure build-up during manufacturing. The inner radius of the core $R_{c,i}$ is set at 9 mm in accordance with Koch's methodology [33]. The density ρ_c of the core results from the densities of the sub-components according to the rule of mixture. In this case, the density of the silicone rubber type 3 HB from TFC is $\rho = 1170 \text{ kg/m}^3$ and the density of the lead is $\rho = 11350 \text{ kg/m}^3$. The selected volume content of the lead balls in the silicone rubber is $\phi_{\text{fill}} = 50\%$. The lead balls were added to increase the elastic core's overall density and, consequently, the exerted pressure while rotating. The volume content was selected based on empirical values derived from previous studies on producing polygonal cross-sections because this method results in a uniform distribution of the lead balls [33]. The additional pressure of the core due to the rotation in the process can now be calculated using the determined geometry of the elastic core. The total pressure in the process for each layer is calculated by adding the centrifugal forces of the core and the inner layers of the preform. This leads to a pressure of 16000 Pa during manufacturing of the part at $n = 3300 \text{ rpm}$ in the presented work. Based on this approach the achievable pressure for five different diameters namely 40, 60, 80, 100 and 120 mm with identical wall thickness of 2.5 mm and an elastic core with a normalized wall thickness of 0.47 are calculated. The results are presented in Figure 16 for different rotational speeds. The achieved consolidation pressure of the demonstrated rotational molding process is quite low, compared to the 8 bars of consolidation pressure in the BAM process. A pressure of 8 bar can be achieved in rotational molding for a part with a diameter of 100 mm at a rotational speed of 9000 rpm. This theoretical analysis shows that high pressures similar to BAM can be achieved by rotational molding with an elastic core for bigger diameters and high rotational speed. Unfortunately, this was not feasible in the present work due to the limitations of machinery.

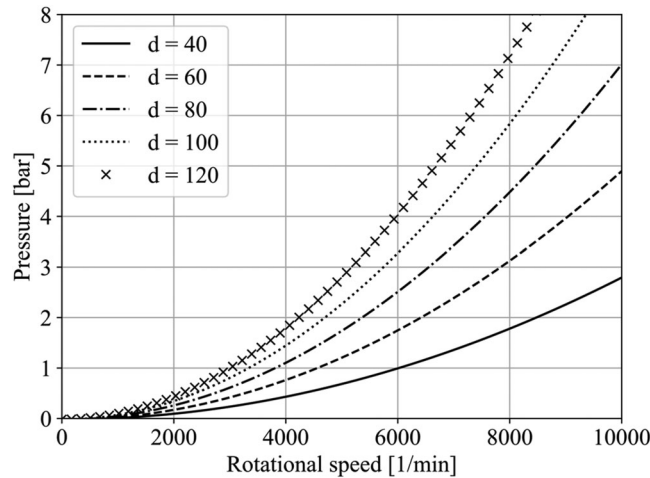


Figure 16. Comparison of the achievable pressures with an elastic core at different component diameters and speeds in rotational molding.

3.4. Bladder assisted molding (BAM)

Figure 17 shows the curved demonstrator which was consolidated in a BAM process. The surface is fully molded on the intrados, extrados and neutral area. A flash can be seen at the intrados and extrados at the parting line of the multipiece-mold. Due to the application of internal pressure by the bladder system, the diameter of the preform expands and the fibers are loaded during consolidation which minimizes in-plane fiber wrinkling.

In CT-scanning the physical dimensions of the complete hollow profile would have exceeded the optimal sample size for achieving the required spatial resolution. Therefore, a smaller segment of the curved hollow profile (see Figure 18a) was scanned in CT, ensuring the inclusion of the halfway point A-A of the curve where differences between intrados and extrados are expected to be at their maximum. The CT scan revealed that the cross section along the profile axis is without any major voids or defects indicating a good consolidation quality of the composite. The wall thickness was evaluated from the cross-section depicted in Figure 18b, which was defined orthogonal to the center line of the profile. Multiple measurements were taken in intervals of 45° around the profile cross-section, beginning at the intrados (0°), passing through the neutral line (90°), reaching the extrados (180°), and continuing back around to the intrados (360°).

A significant deviation in wall thickness between the extrados and intrados was observed, with a difference of approximately 1.04 mm, corresponding to roughly 53%. This difference can be attributed primarily to differences in the cover factor between these two regions. Figure 19 illustrates the relationship between cover factor and wall thickness. At the extrados the lower cover factor value signifies less tape material and more gaps in the braided architecture when compared to the intrados resulting in a lower



Figure 17. Curved demonstrator manufactured by BAM (a); Detailed view of the intrados (b); Detailed view of the extrados (c).

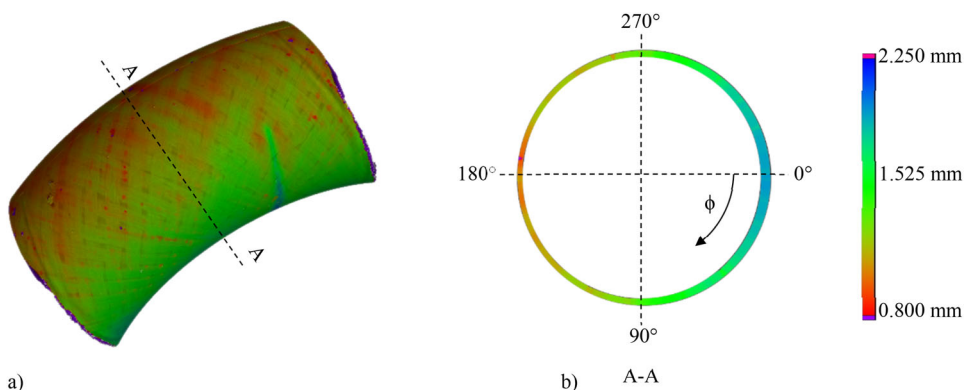


Figure 18. CT scan of the curved tube segment (a); cross-section for wall thickness analysis (b).

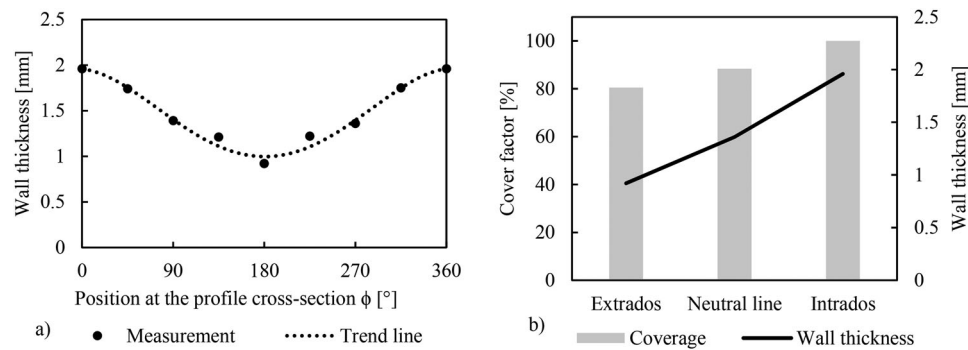


Figure 19. Measured wall thickness variance of the profile from extrados to intrados (a) and comparison to the measured cover factor (b).

wall thickness. It should be noted that this comparison is only of qualitative nature, since the cover factor was only measured on the first braided layer. The consolidated curved profile consists of eight braided layers with a non-negligible difference in diameter between the outermost and innermost layer. The diameter has a significant influence on the cover factor and the effects of the gaps within the braid architecture stack with increasing layer count.

These results demonstrate the possibility of consolidating near-net shape tape-braided preforms in the BAM process. Due to the processes of curved preforming and BAM being auxiliary material intensive, only two demonstrators were manufactured in total. The results shown in Figure 19 are based on measurements taken from the first demonstrator. To ensure the displayed wall thickness trajectory along the circumference of the profile is representative, wall thickness values were extracted from two more cross-section near the vertex of the curved hollow profile, all of which closely followed the depicted trajectory. A coarse CT scan was used to analyze the second demonstrator, which confirmed the observed trends. While for this demonstrator a substantial difference in wall thickness from extrados to intrados was observed, depending on the application the demonstrated process route may be acceptable. Compared to a previous study on bend forming tape-braided profiles, the fiber angle distribution observed in this work expressed a contrary trend from intrados to extrados. In [17], the bend-forming process of a CF/PA6 tube with a braid architecture of $\pm 50^\circ$ was investigated and the resulting fiber angles showed a decreasing trend from intrados to extrados. In contrast, for the curved braiding process in this study, an increase in fiber angles, especially from the intrados to the neutral line, was observed. These results suggest contrary trends in the resulting braid architectures of these processes for curved profiles. However, further investigation of comparable profiles with identical targeted braid architectures is required to draw a conclusion on the fiber angle distributions achievable by these process routes. Additionally, the interaction of the braid angle and the cover factor with the resulting wall thickness of the profile needs to be experimentally investigated and numerically modelled on all layers of a preform taking into account the changes in diameter from the innermost to the outermost layer of a braided hollow profile to improve the predictive capabilities of the numerical approach.

4. Conclusion

This work investigates two novel processing routes for manufacturing braided hollow profiles from CF/PA6 tapes, focusing on preforming, consolidation, and quality evaluation of the resulting profiles. For straight preforms, the braiding process was characterized and shown to be well understood, with analytical models effectively predicting braid architecture [28,29]. In contrast, the development of a near-net-shape curved preform presented unique challenges, including designing a mandrel for non-destructive demolding of the preform and preventing tape-mandrel-collision during the braiding operation. A lost core approach was realized by 3D printing the mandrel using a water-soluble PVA filament. The collision of incoming tapes with the mandrel could be addressed by a double guide ring setup that deflects the tapes steeply at the deposition point moving them out of the mandrel range. In future work, investigating different demolding strategies for curved preforms, such as foldable mandrels could significantly improve production times and minimize the amount of auxiliary material for curved braided profiles.

The software BRAIDSIM developed at the University of Twente was used to predict the resulting braid architecture based on the input process parameters and the results were compared to the experimental investigations. The software accurately predicted the fiber angle and cover factor measured on the straight preform with deviations for the fiber angles limited to 2.42% and the cover factor to 1.62%. For the curved preform, predicted cover factor values at the extrados, neutral line and intrados were in good agreement with the experiments with deviations limited to a maximum of 5%. However, a significant underestimation of the measured fiber angles of approximately 11–14% was observed. Further research is required to enhance the numerical design of curved tape-based braiding processes. This should include parameter studies to identify different mandrel curvature to diameter ratios at which the current BraidSim approach shows an acceptable prediction accuracy. The implementation of friction models that include yarn-yarn and yarn-guide ring interactions, as well as utilization of FEM techniques to include the non-negligible bending stiffness of fiber-reinforced thermoplastic tapes, could further improve the numerical approach.

The straight preform was consolidated in the rotational molding process using a modified turning center with an integrated heat chamber. In addition, an elastic core was introduced to increase the pressure during manufacturing. Results from the CT scan of the manufactured part indicate a wall thickness of 1.22 mm after consolidation. However, the innermost layer was not fully consolidated. This phenomenon occurred on opposite sides and suggests an insufficient and uneven pressure distribution. Theoretical calculations demonstrated that higher profile diameters and rotational speeds increase the achievable consolidation pressure and thus could improve the consolidation quality. In future research, the validation of these theoretical calculations should be prioritized. This can be achieved by expanding existing machinery to enable higher rotational speeds and by identifying suitable diameters at different speeds at which the consolidation quality is acceptable.

For the curved preform, BAM using a multi-piece tool and a silicone bladder at 8 bar pressure achieved good surface quality and minimal fiber wrinkling. Analysis by CT scanning revealed a good consolidation quality, without any major voids or defects within the composite. A significant difference in the wall thickness of the consolidated profile between the intrados and the extrados was observed on the CT scan. This difference in wall thickness is mainly attributed to the differences in cover factor that were predicted in simulation as well as observed on a single braid layer. The results demonstrate the potential of the novel process route, to manufacture curved braided profiles with a high quality and without the additional processing step of bend forming a straight profile after consolidation. Further research is needed to identify the relationship of the curvature to diameter ratio of curved profiles and the resulting wall thickness variance between the extrados and the intrados. Additionally, the investigation of methods to locally enhance the ply count or coverage is a subject of interest. Potential approaches include the use of patching or the application of preforming utilizing automated fiber placement. A comprehensive understanding of the relationship between coverage, ply count, and resulting wall thickness is imperative for local preform modifications. To achieve this, numerical and experimental parameter studies are necessary. Furthermore, a comprehensive comparison of the resulting braid architecture from the bend forming process and the curved braiding process should be conducted, as the results of this study suggests a divergent trend between these processes.

Acknowledgement

The authors thank the Production Technology Group of the University of Twente for providing access to the BRAIDSIM software.

Disclosure statement

No potential conflict of interest was reported by the authors.

Funding

The authors gratefully acknowledge the funding of this work by the German Research Foundation, DFG, within the research and knowledge transfer project 'Multi-functional high-performance profile systems in intrinsically manufactured fiber-reinforced metal hybrid construction (ProMi)' with Grant No. GU 614/28-1 445506821.

ORCID

Eric Mischorr  <http://orcid.org/0009-0007-5957-3566>

Data availability statement

The data that support the findings of this study are available from the corresponding author, Eric Mischorr, upon reasonable request.

References

1. European Environment Agency. Greenhouse gas emissions from transport in Europe | European Environment Agency's home page. April 03, 2025. Available from: <https://www.eea.europa.eu/en/analysis/indicators/greenhouse-gas-emissions-from-transport>.
2. Fleischer J. Intrinsische Hybridverbunde für Leichtbautragstrukturen. Berlin, Heidelberg: Springer Berlin Heidelberg; 2021.
3. Krueger R, Bergan A. Advances in thermoplastic composites over three decades - A Literature Review. NASA STI Program Report Series. 2024. NASA-ID: NASA/TM-20240005376.
4. Kwon B, Choi W, Ju H, et al. Effects of consolidation processing parameters on the surface morphology and void content of braided thermoplastic composite tubes. *Funct. Compos. Struct.* 2021;3(3):e035004. doi: [10.1088/2631-6331/ac199f](https://doi.org/10.1088/2631-6331/ac199f).
5. Alshammari BA, Alsuhybani MS, Almushaikeh AM, et al. Comprehensive review of the properties and modifications of carbon fiber-reinforced thermoplastic composites. *Polymers*. 2021;13(15):2474. doi: [10.3390/polym13152474](https://doi.org/10.3390/polym13152474).
6. Mărieș GRE, Abrudan AM. Thermoplastic polymers in product design. *IOP Conf Ser Mater Sci Eng.* 2018;393:e012118. doi: [10.1088/1757-899X/393/1/012118](https://doi.org/10.1088/1757-899X/393/1/012118).
7. Brasington A, Sacco C, Halbritter J, et al. Automated fiber placement: a review of history, current technologies, and future paths forward. *Composites Part C.* 2021;6:100182. doi: [10.1016/j.jcomc.2021.100182](https://doi.org/10.1016/j.jcomc.2021.100182).
8. Yassin K, Hojjati M. Processing of thermoplastic matrix composites through automated fiber placement and tape laying methods. *J Thermoplast Compos Mater.* 2018;31(12):1676–1725. doi: [10.1177/0892705717738305](https://doi.org/10.1177/0892705717738305).
9. Minchenkov K, Vedernikov A, Safonov A, et al. Thermoplastic pultrusion: a review. *Polymers*. 2021;13(2):180. doi: [10.3390/polym13020180](https://doi.org/10.3390/polym13020180).
10. Andrae M. Composite Pipes and Fittings for Aero-Engines Dressing 2016. 12 September, 2016; [cited 2025 Apr 01]. Available from: <https://cordis.europa.eu/project/id/323514/reporting>.
11. von HJ, Grohmann Y, Khan S. Methods for the post-consolidation of high-speed-wound thermoplastic CFRP tubes. In: Christophe Binetruy, Jacquemin F, editors. *Proceedings of the 21st European Conference on Composite Materials*. Nantes Université; 2024, p. 698–705.
12. Nieschlag J, Ruhland P, Coutandin S, et al. Rotational molding for the production of hybrid FRP metal tension and compression rods with form fit. In *Production at the leading edge of technology*. Berlin, Heidelberg: Springer Vieweg; 2019. p. 131–138.
13. Ehleben M, Schürmann H. Manufacturing of centrifuged continuous fibre-reinforced precision pipes with thermoplastic matrix. *Compos Sci Technol.* 2006;66(15):2601–2609. doi: [10.1016/j.compscitech.2006.03.015](https://doi.org/10.1016/j.compscitech.2006.03.015).
14. Barfuss D, Würfel V, Grützner R, et al. Integral blow moulding for cycle time reduction of CFR-TP aluminium contour joint processing. In: author(s); 2018, p. 50003.
15. Cherif C. *Textile Werkstoffe für den Leichtbau*. Berlin, Heidelberg: Springer Berlin Heidelberg; 2011.
16. Barfuss D, Grützner R, Garthaus C, et al. Intrinsic manufacture and design of positive locking fibre reinforced thermoplastic metal hollow structures. In *Proceedings of the 17th European Conference on Composite Materials: ECCM17 – 17th European Conference on Composite Materials*, 26–30th June 2016. Munich, Germany. Augsburg: MAI Carbon Cluster Management GmbH; 2016.
17. Eckardt S, Barfuß D, Condé-Wolter J, et al. Study on bend-forming behaviour of thermoplastic tape-braided CFRTP profiles. In: *Tagungsband SAMPE Europe Conference*; 2020.
18. Monnot P, Lévesque J, Laberge Lebel L. Automated braiding of a complex aircraft fuselage frame using a non-circular braiding model. *Composites Part A.* 2017;102:48–63. doi: [10.1016/j.compositesa.2017.07.011](https://doi.org/10.1016/j.compositesa.2017.07.011).
19. Czichos R, Bareiro O, Pickett AK, et al. Experimental and numerical studies of process variabilities in biaxial carbon fiber braids. *Int J Mater Form.* 2021;14(1):39–54. doi: [10.1007/s12289-020-01541-4](https://doi.org/10.1007/s12289-020-01541-4).
20. van Ravenhorst JH. Design tools for circular overbraiding of complex mandrels. Enschede: University of Twente; 2018. doi: [10.3990/1.9789036545860](https://doi.org/10.3990/1.9789036545860).
21. van Ravenhorst JH, Akkerman R. Circular Braiding Process Simulation for a Pressure Vessel. In: *Volume 6A: Materials and Fabrication*. Anaheim, California, USA: American Society of Mechanical Engineers; 2014.
22. van Ravenhorst JH, Akkerman R. A yarn interaction model for circular braiding. *Compos Part A: Appl Sci Manufact.* 2016;81:254–263. doi: [10.1016/j.compositesa.2015.11.026](https://doi.org/10.1016/j.compositesa.2015.11.026).
23. Vu AN, Grouve W, Akkerman R. Modeling of yarn interactions for non-axisymmetric biaxial overbraiding simulations. *Composites Part A Appl Sci Manufact.* 2023;167:107421. doi: [10.1016/j.compositesa.2022.107421](https://doi.org/10.1016/j.compositesa.2022.107421).

24. Vu AN, Grouve W, Warnet LL, et al. Modeling anisotropic friction in triaxial overbraiding simulations. *Compos Part A: Appl Sci Manufactur*. 2024;177:107958. doi: [10.1016/j.compositesa.2023.107958](https://doi.org/10.1016/j.compositesa.2023.107958).
25. Anderson JP, Altan MC. Properties of composite cylinders fabricated by bladder assisted composite manufacturing. *Trans ASME J Eng Mater Technol*. 2012;134(4):17. doi: [10.1115/1.4007017](https://doi.org/10.1115/1.4007017).
26. Würfel V, Condé-Wolter J, Pietsch AL, et al. Investigation of variothermal mould heating systems for processing of high temperature thermoplastic composites in short cycles. 2022.
27. Celanese Materials Database. Datasheet CELSTRAN[®] CFR-TP PA6 CF60-03; 2024.
28. Rosenbaum JU. Flechten: rationelle Fertigung faserverstärkter Kunststoffbauteile. ZuglAachen, Techn. Hochsch., Diss. 1990 u.d.T.: Rosenbaum, Jens Ulrich: fertigung von faserverstärkten Kunststoffbauteilen unter Einsatz der Flechttechnik. Köln: verl. TÜV Rheinland; 1991.
29. Kyosev Y. Braiding technology for textiles: principles, design and processes. Amsterdam: Elsevier; 2015.
30. Geuzaine C, Remacle J-F. Gmsh: A 3-D finite element mesh generator with built-in pre- and post-processing facilities. *Numerical Meth Eng*. 2009;79(11):1309–1331. doi: [10.1002/nme.2579](https://doi.org/10.1002/nme.2579).
31. Grosse-Brauckmann K. On gyroid interfaces. *J Colloid Interface Sci*. 1997;187(2):418–428. doi: [10.1006/jcis.1996.4720](https://doi.org/10.1006/jcis.1996.4720).
32. Gröger B, Gerritzen J, Eckardt S, et al. Modelling of composite manufacturing processes incorporating large fibre deformations and process parameter interactions: Example braiding. In *ICCM*; 2023, p. 245.
33. Fleischer J, Koch S-F, Coutandin S. Manufacturing of polygon fiber reinforced plastic profiles by rotational molding and intrinsic hybridization. *Prod Eng Res Devel*. 2015;9(3):317–328. doi: [10.1007/s11740-015-0620-0](https://doi.org/10.1007/s11740-015-0620-0).
34. Kunz J, Studer M. Determining the modulus of elasticity in compression via the Shore A Hardness. In *Kunststoffe international*. München: Carl Hanser Verlag; 2006. p. 92–94.